Manuscript

Urban Analytics and City Science

EPB: Urban Analytics and City Science
2024, Vol. 0(0) 1–14

DOI: 10.1177/23998083241274391
journals.sagepub.com/home/epb
Sage

Mapping pedestrian network level outdoor heat hazard distributions in Philadelphia

Xiaojiang Li
University of Pennsylvania, USA

Abstract

With the rise of global temperature, many cities are suffering from more and more frequent extreme heat in hot summers. Quantitative information on the spatial distributions of urban heat has become more and more important for extreme heat mitigation and adaptation in cities. This study first investigated the fine-level heat hazard distributions at the sidewalk and building block level from the pedestrian perspective in Philadelphia, Pennsylvania. The urban microclimate modeling based on a high-resolution urban geometrical model was used to generate the 1m resolution outdoor heat hazard map in the study area. The sidewalk map was overlaid on the generated high-resolution heat hazard map to estimate the sidewalk level heat hazard. Based on the sidewalk level heat hazard map, this study further calculated the heat hazard level in the 400m walkshed along sidewalks for each building block. The building level hazard data were then aggregated at the census tract level to compare with the socioeconomic and racial/ethnic variables. The result shows that neighborhoods with higher proportion of African Americans have a higher heat hazard level in Philadelphia. This study would provide new insights for developing more thermally comfortable and pedestrian-friendly neighborhoods in the context of climate change.

Keywords

Urban heat distribution, urban microclimate modeling, pedestrian level heat hazard, walkshed

Introduction

Extreme heat events are increasing in frequency in large U.S. cities and are responsible for a greater annual number of climate-related fatalities (Borden and Cutter 2008; Stone et al., 2010). Extreme heat events have led to mortality increase in many cities all over the world, and many cities expect extreme heat events more often because of urban heat island effects and climate change (Alexander

Corresponding author:
Xiaojiang Li, Department of City and Regional Studies, University of Pennsylvania, 210 S 34th St, Philadelphia, PA 19104, Philadelphia, Pennsylvania, 19104-6243, USA.
Email: lixiaojiang.gis@gmail.com

Data Availability Statement included at the end of the article

and Arblaster, 2009; Gabriel and Endlicher, 2011). These summer heat waves will also increase the deaths and illness caused by infectious disease and air pollution (Easterling et al., 2000; McPhearson et al., 2020; Patz et al., 2005). In addition, heat stress deteriorates the livability and walkability of cities (Lee et al., 2013) and impacts human physical activity levels.

It is important to examine how urban residents are exposed to extreme heat in cities in order to take measures to mitigate the health risks of extreme heat (Li and Wang, 2021). Knowing the spatial distribution and the temporal variation of heat is of great importance to understand how people are exposed to extreme heat (Hsu et al., 2021; Li, 2021; Reid et al., 2009). Unlike dense ground-based weather station networks, which are rare in cities, satellite-derived land surface temperature (LST) provides an efficient way to map the spatial distribution of urban heat at a large scale. While being widely used in urban heat mapping, LST cannot present the human-centric and pedestrian-level heat exposure in cities because of the coarse resolution and fixed observation periods. In addition, the LST is impacted significantly by the temperature of building roofs and treetops, which are not the place of human activities. Other than temperature, human heat stress is also impacted by other factors, such as solar and terrestrial radiation, shade, wind, and humidity (Klemm et al., 2015; Li, 2021; Li and Wang, 2021; Norton et al., 2015). For example, a person directly exposed to solar radiation gets significantly more heat exposure than someone staying in the shade. However, both LST and air temperature cannot account for these factors.

There are still few studies that examine the heat exposure at individual level. Karner et al. (2015) examined the heat exposure of non-motorize travel in the San Francisco Bay Area using the transportation activity data and 1 km resolution air temperature from the *Daymet* data. Li et al. (2023) applied a simulated travel pattern to estimate the heat exposure of travelers in Phoenix, Arizona. The heat metrics of mean radiant temperature and wet bulb globe temperature were calculated based on the meteorological parameters from the *Daymet* data. However, most of those heat metrics are too coarse to fully indicate the spatial distribution of heat exposure within the urban space, where heat exposure varies significantly street by street because of the heterogenous urban landscapes (Li, 2021).

Fine-level microclimate modeling based on high-resolution, three-dimensional urban geometrical models, and local meteorological data provides a more comprehensive way to examine outdoor heat exposure at pedestrian level (Li, 2021; Li and Wang, 2021; Lindberg et al., 2008; Lindberg et al., 2016; Lindberg and Grimmond, 2011; Maronga et al., 2015; Matzarakis et al., 2007). Based on the high-resolution input urban geometrical model, it is possible to calculate human heat stress indicators at the meter level. For example, solar irradiance geometry models can estimate pedestrian level heat exposure through a human-centric point of view based on urban geometrical models and meteorological data. Ultimately, the finer-resolution heat hazard information would provide unprecedentedly detailed understanding of the heat exposure on pedestrians and the mechanism of how extreme heat events impact human wellbeing.

However, there are still few studies that use urban microclimate modeling for city-scale analyses (Kong et al., 2022; Li, 2021; Li and Wang, 2021). The high computational cost of radiation simulations on high-resolution urban geometrical models is the major obstacle. Recently, Li and Wang (2021) developed GPU-accelerated algorithms for urban microclimate modeling that can efficiently generate 1m resolution hourly mean radiant temperature (T_{mrt}) maps at large scales based on urban geometrical models derived from LiDAR and aerial imagery. In this study, we adopted the efficient urban microclimate modeling and mapped a 1m resolution T_{mrt} map in Philadelphia. Based on the 1m resolution urban heat hazard map, this study evaluated the heat hazard at the sidewalk level and then examined the heat hazard of the walkshed of each building block. Please note that the walkshed only includes the potential paths for people living in the buildings; therefore, the heat hazard of walksheds cannot fully indicate the actual heat exposure at pedestrian level, since the mobility of pedestrians is not considered. This study further investigated pedestrian level heat hazard among different socioeconomic and racial/ethnic groups in Philadelphia. This study provides

an unprecedented, detailed understanding of heat hazard at the pedestrian level, which would help to develop walkable cities and build resilience to extreme heat in the context of climate change.

Methodology

Study area and data preparation

The study area is in Philadelphia, Pennsylvania, USA (Figure 1). The datasets used in this study include the high-resolution (1m) land-use map, sidewalk map, building footprint map, LiDAR cloud

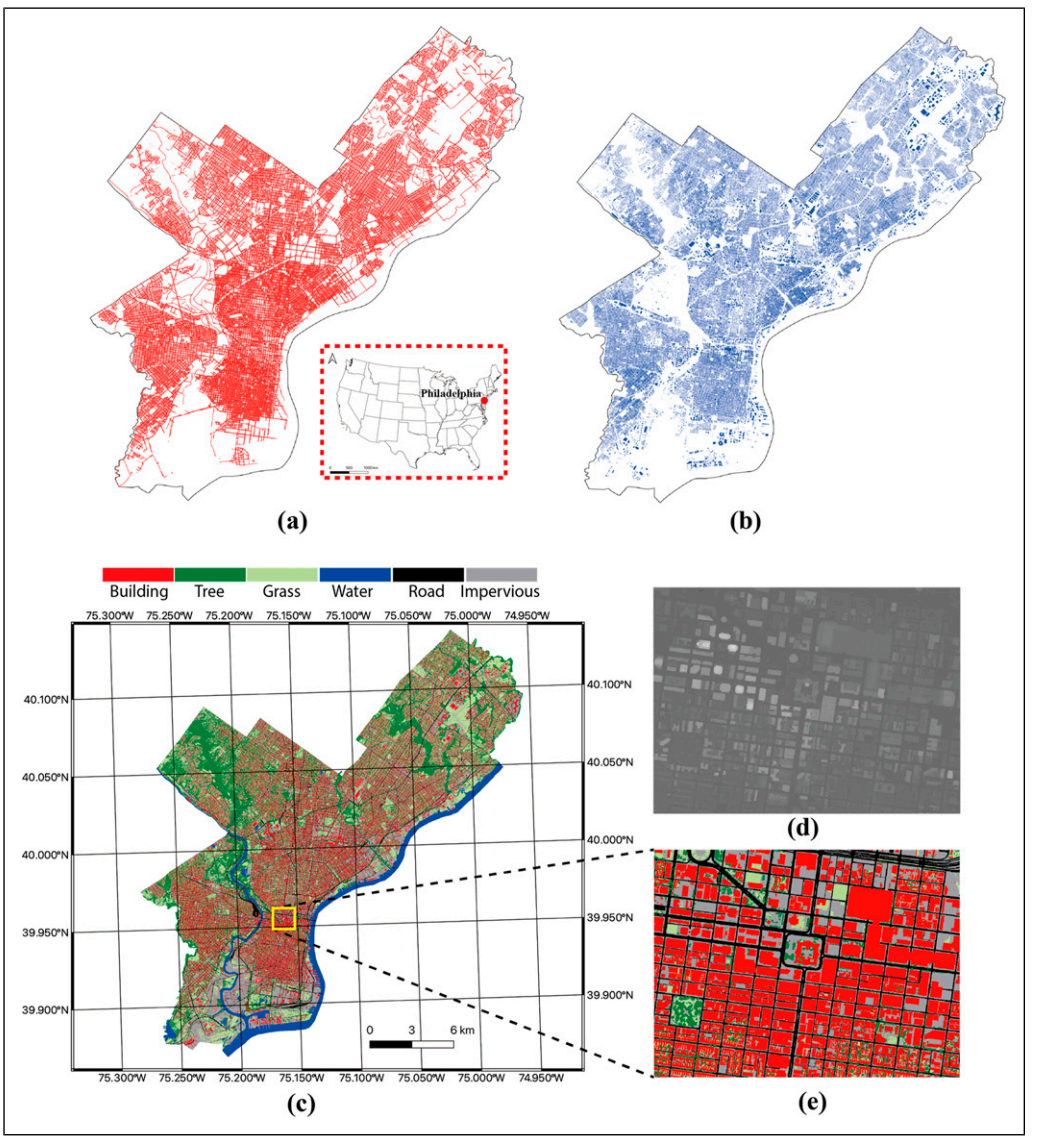

Figure 1. Location and datasets used in the study area: (a) the sidewalk map, (b) the building footprint map, (c) the fine-level resolution land-use data in Philadelphia, (d) the normalized digital surface model of the downtown Philadelphia, and (e) the land-use map in the downtown of the Philadelphia.

point data, and meteorological data (Figure 1). The high-resolution land-use map created semi-automatically based on high-resolution aerial imageries and LiDAR data with accuracy as high as 90% was collected from Pennsylvania Spatial Data Access (PASDA, https://www.pasda.psu.edu/). The high-resolution LiDAR data in the form of pre-processed x, y, and z point cloud files were collected from the United States Geological Survey 3D Elevation Program (https://usgs.entwine.io/). In this study, the open-sourced tool PDAL was used to convert the LiDAR cloud points into digital elevation model (DEM) and digital surface model (DSM) automatically. The high-resolution land-use map and the generated DSM were combined to generate the building height model and the tree canopy height model. In addition, this study collected the sidewalk map in Philadelphia from DVRPC (Delaware Valley Regional Planning Commission, https://walk.dvrpc.org/). The hourly meteorological data of air temperature, humidity, global horizontal radiation, direct radiation, and diffuse radiation was collected from the National Renewable Energy Laboratory (NREL) (https://nsrdb.nrel.gov/). The building footprint map was collected from Microsoft building footprint database. The land-use information for each building block was determined by the overlay of the building footprint on the land-use map of the study area.

Mean radiant temperature estimation

This study used the SOlar and LongWave Environmental Irradiance Geometry (SOLWEIG) model to calculate and map the spatio-temporal distribution of mean radiant temperature (T_{mrt}). The high-resolution urban geometrical model was used to represent the fine-level urban landscape. The T_{mrt} is an objective indicator of the human body's radiation exposure with consideration of the solar radiation fluxes, air temperature, and shade. The SOLWEIG model has been developed over decades and validated worldwide. In the SOLWEIG model, the T_{mrt} can be calculated as follows: (Lindberg et al., 2008; Lindberg and Grimmond, 2011)

$$T_{mrt} = \sqrt[4]{R/\varepsilon_p \sigma} - 273.15 \tag{1}$$

where σ is the Boltzmann constant, ε_p is the emissivity of the human body (standard value 0.97), and R is the radiation that a human body exposed and can be estimated as,

$$R = \xi_k \sum_1^6 K_i F_i + \varepsilon_p \sum_1^6 L_i F_i \tag{2}$$

where K_i is the shortwave radiation component from six directions (north, south, west, east, top, and bottom), L_i is the longwave radiation, F_i is the angular factor between a person and the surrounding environment, and ξ_k is the absorption coefficient for shortwave radiation (standard value 0.7). Figure 2(a) shows the process of T_{mrt} estimation based on the local meteorological data, tree canopy height model, and building height model.

The SOLWEIG model is very slow running on the CPU based on high-resolution urban geometrical models (Li, 2021; Li and Wang, 2021). This study adopted the previously developed GPU-based method to accelerate the SOLWEIG model (Li and Wang, 2021). The GPU-parallel computing algorithm has been reported to achieve a speed as high as 400,000 times for urban geometrical parameter estimation than the regular method (Li and Wang, 2021). In this study, the GPU-accelerated algorithm for estimating the T_{mrt} can achieve a 100x speedup compared with the regular method. Figure 2(b) shows the computational model of the GPU-accelerated model for computing the T_{mrt} based on the input urban geometrical model and the meteorological data.

In this study, the meteorological data for the summertime of 2019 was used to generate the hourly T_{mrt} maps of summertime from July 1st to Sep 1st from 9 a.m. to 4 p.m. each day, which are

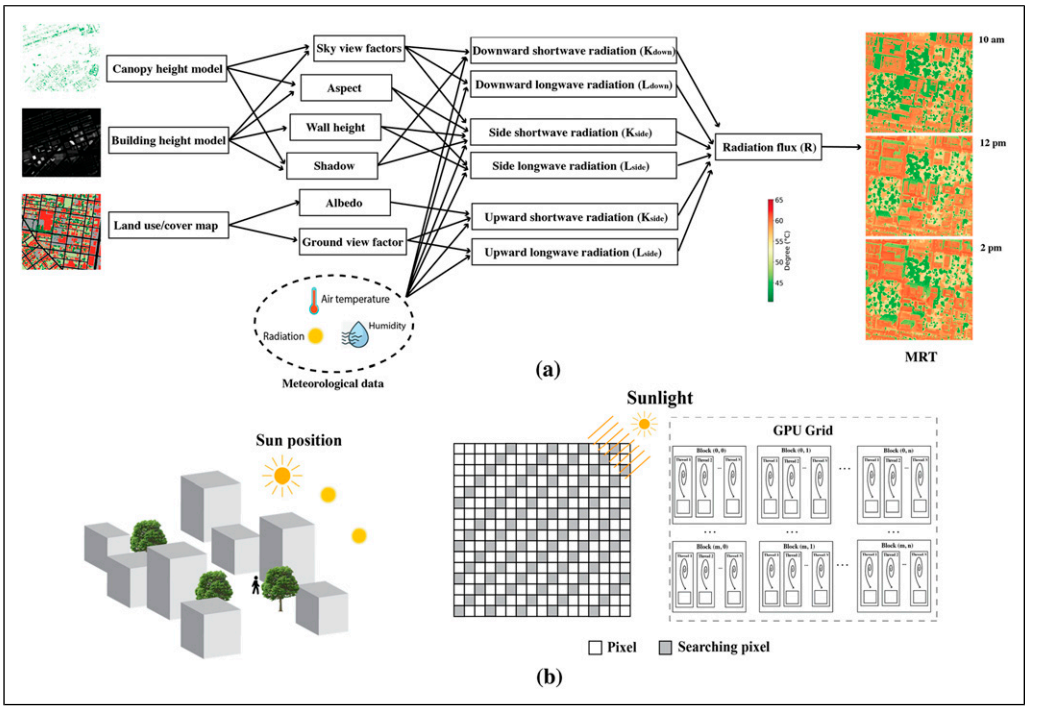

Figure 2. Calculation of the mean radiant temperature (T_{mrt}) using the SOLWEIG model based on land-use map, urban geometrical model, and meteorological data using the GPU-accelerated algorithm: (a) the SOLWEIG model for estimating the T_{mrt} and (b) the GPU parallel computing framework for modeling radiation fluxes in complex urban geometrical spaces based on building height model and tree canopy height model in raster data format.

considered as the hottest time periods of 1 year. To generate the general spatial distribution of the heat hazard in the study area, those hourly T_{mrt} maps were aggregated by the mean value.

Estimating heat hazard level along sidewalk

In order to generate the heat hazard along the sidewalks, this study overlaid the sidewalk map on the generated 1 m resolution urban heat hazard map to calculate the heat hazard along sidewalks. The sidewalk map was planarized based on the intersection points into segments. Figure 3(a) and (b) shows the overlay of the sidewalk segments on the generated 1 m resolution average urban heat hazard map in part of the study area. The open-sourced tool GDAL (Geospatial Data Abstraction Library) was used to conduct the overlay. Then the heat hazard along each sidewalk segment was estimated as the mean values of all T_{mrt} pixels along the segment.

Based on the sidewalk level heat hazard map, this study further estimated the heat hazard for each building block within walkshed of a 400m walking distance, which is usually considered as the general walking distance threshold. The centroid of each building footprint was used as the origin to determine the walkshed (Figure 3(c)). Then the walking heat hazard level for each building was estimated by averaging the heat hazard along all the planarized sidewalk segments in the walkshed (Figure 3(d)) as follows:

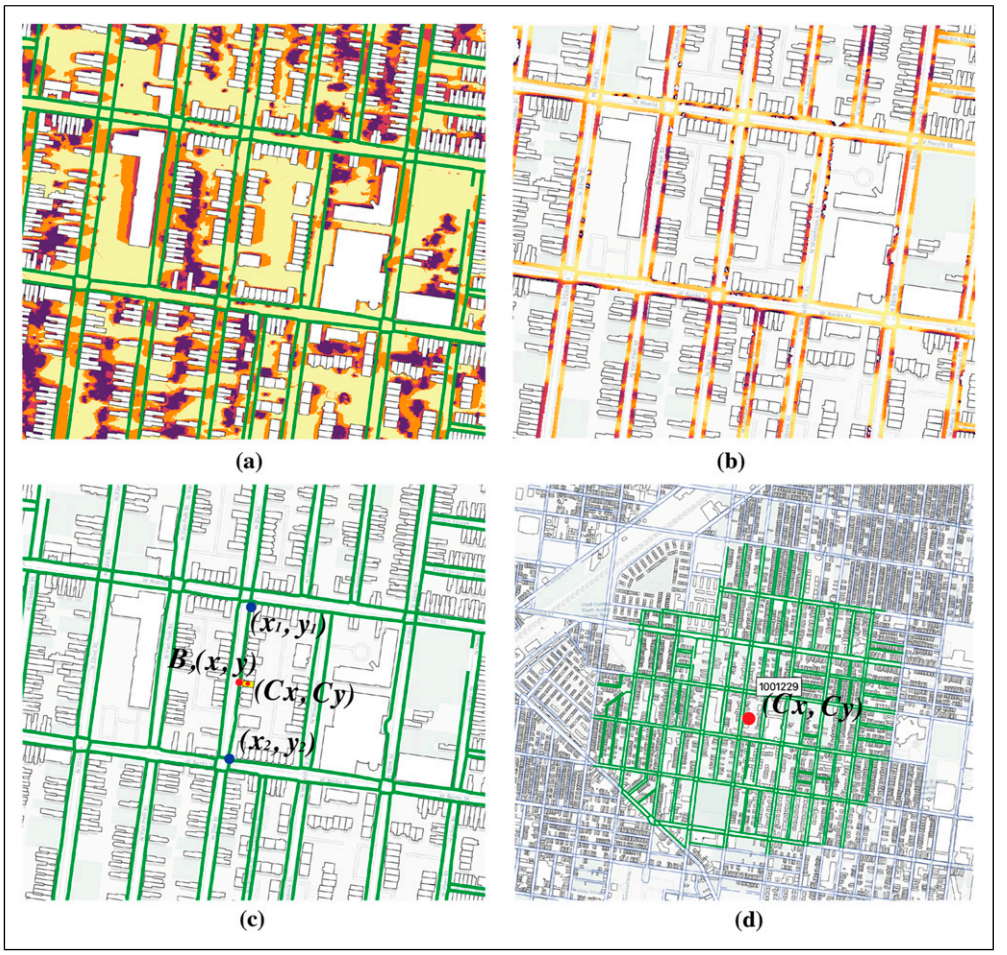

Figure 3. Estimation of heat hazard along the sidewalk and building level heat hazard: (a) the overlay of the sidewalk map on the generated pixel level T_{mrt}, (b) the heat hazard along the sidewalk, (c) the front-end point along street of one building in the study area, and (d) the sidewalk segments in 400m walkshed of one building block.

$$HeatExpo = \sum_{i=0}^{n} Heat_i \tag{3}$$

where n is the number of planarized sidewalk segments within the walkshed of 400 walking distance and *Heat* is the heat hazard along the ith sidewalk segment within the walkshed. In this way, we estimated the heat hazard at the building block level in the study area.

The distance between building and nearby sidewalk segments was calculated as the network distance while generating the walkshed of each building. The frontend point of each building is deterred as the perpendicular distance from the centroid of the building footprint to the closest sidewalk segment (Figure 3(c)). The coordinate of the frontend point $B\,(x, y)$ of each building block with the centroid of (C_x, C_y) was calculated using liner interpolation process based on the coordinate of the two endpoints (x_1, y_1) and (x_2, y_2) of the sidewalk segment.

Social-environmental analyses

In order to examine the pedestrian level heat hazard among different socioeconomic and racial/ethnic groups, this study compared the aggregated building level heat hazard map with socio-economic and racial/ethnic statuses in the study area. To represent the social statuses of residents, this study selected variables of per capita income, proportion of non-Hispanic Whites, proportion of African Americans, proportion of Hispanics, proportion of Asian Americans, proportion of people older than 65, proportion of people younger than 5, proportion of people with bachelor or higher degrees, and proportion of people without high-school degrees based on previous studies (Hsu et al., 2021; Landry and Chakraborty, 2009; Li, 2021). All the variables were collected from American Community Survey 5-year data of 2015–2019. To make the heat maps comparable to the census data, this study aggregated building level heat hazard map to census tract using the mean value.

Correlation analysis was conducted to compare the correlation between heat hazard and social variables. The ordinary least squares (OLS) regression models were applied to investigate the associations between the social variables and heat hazard level. Only those variables with significant correlation with the heat hazard levels were selected in the OLS regression model. The global Moran's *I* statistics were used to examine the spatial autocorrelation in the residuals of the OLS regression model. The spatial regression model was then applied when the residuals have significant spatial dependence in the OLS model.

There are two major methods to incorporate the spatial dependence into the regression model: spatial lag regression model (SAR_{lag}) and spatial error regression model (SAR_{err}). The SAR_{lag} incorporates the spatial dependence into the dependent variable, while the SAR_{err} incorporates the spatial dependence into the error terms. In this study, the *PySal* module was used to conduct the spatial regression analyses (Rey and Anselin, 2009), and the Lagrange Multiplier and Robust Lagrange Multiplier tests were conducted to judge whether to use SAR_{lag} model or SAR_{err}.

Results

Figure 4(a) and 4(b) show the spatial distributions of the mean radiant temperature (T_{mrt}) at the pixel level and the sidewalk in the city of Philadelphia for the summer of 2019. Generally, the T_{mrt} along the sidewalk (Figure 4(b)) has a similar pattern to the pixel level T_{mrt} map (Figure 4(a)). The downtown areas and the northwestern areas have lower T_{mrt}, while the northern and northeastern areas have a higher T_{mrt}. These spatial patterns match well with the spatial distributions of tree canopy cover and the high-rise buildings. The downtown area has more high-rise buildings, and the northern and northwestern areas have high tree canopy cover (Figure 1).

Table 1 shows the results of correlation analysis between the heat hazard along the sidewalk and the streetscape variables. The heat hazard has significant and negative correlations with the tree canopy cover, tree canopy height, and building height along sidewalks. The correlations of heat hazard along sidewalks and the landscape features become weaker as the buffer distance increases.

Figure 5 shows the bar chart of the average heat hazard levels for sidewalks with different orientations. The orientation angle starts from the east in anti-clockwise way. The sidewalks with the orientations of 60–90° have significantly lower heat hazard level than sidewalks of other orientation angles. Those streets orient in degree of 0–30 have significantly higher heat exposure level. Figure 6(a) show the spatial distribution of the heat hazard within 400m walking distance walkshed for each building block in the city of Philadelphia. Figure 6(b) shows the aggregated census tract level hazard. Generally, the downtown areas and the northwestern parts of the city have lower heat hazard level, while the northeastern and the southern areas have higher heat hazard level.

Table 2 presents the correlation coefficients between the aggregated building-level heat hazard and the socioeconomic and racial/ethnic variables in the study area at the census tract level. The per

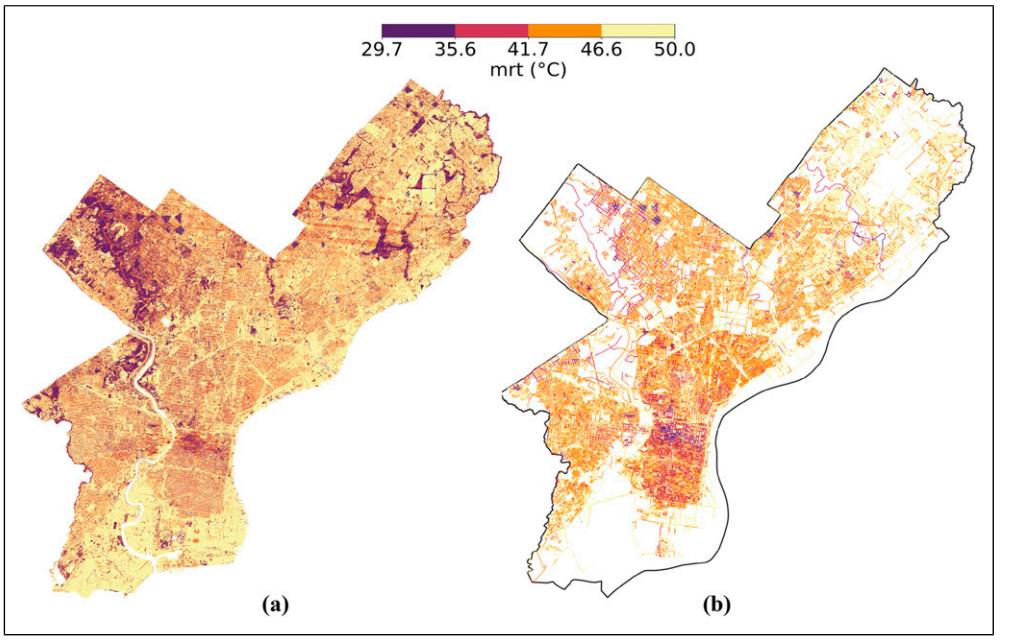

Figure 4. Spatial distributions of the mean radiant temperature (T_{mrt}) at the pixel level (a) and the sidewalk level (b) in Philadelphia.

Table 1. Correlation coefficients between the heat hazard along sidewalk and the nearby landscape variables at different buffer distances.

	Different distances along the sidewalk			
Correlation	10m	20m	30m	*N*
Tree canopy cover	−0.25**	−0.22**	−0.19**	130,962
Height of trees	−0.10**	−0.04**	−0.02**	
Building height	−0.15**	−0.09**	−0.08**	

** Correlation is significant at the 0.01 level (2-tailed).

capita income is strongly and negatively correlated with the heat hazard. The proportion of people with bachelor or higher degrees has no significant correlation with the heat hazard, while the proportion of people without high school degree has a significant and positive correlation with the heat hazard. The proportion of non-Hispanic Whites is significantly and negatively correlated with the heat hazard. The proportion of Hispanics and the proportion of African Americans both are significantly and positively correlated with the heat hazard level, while no significant correlation between the proportion of Asian Americans and heat hazard was detected. The proportion of people under 5 years is significantly and positively correlated with the heat hazard, while the portion of people older than 65 years is not significantly correlated with the heat hazard.

Table 3 presents the regression analysis of the pedestrian level heat hazard and the racial/ethnic and socioeconomic variables. The per capita income is negatively and significantly associated with the building level heat hazard level in the ordinary least squares (OLS) linear regression model, while the association is not significant in the spatial regression model after controlling the spatial

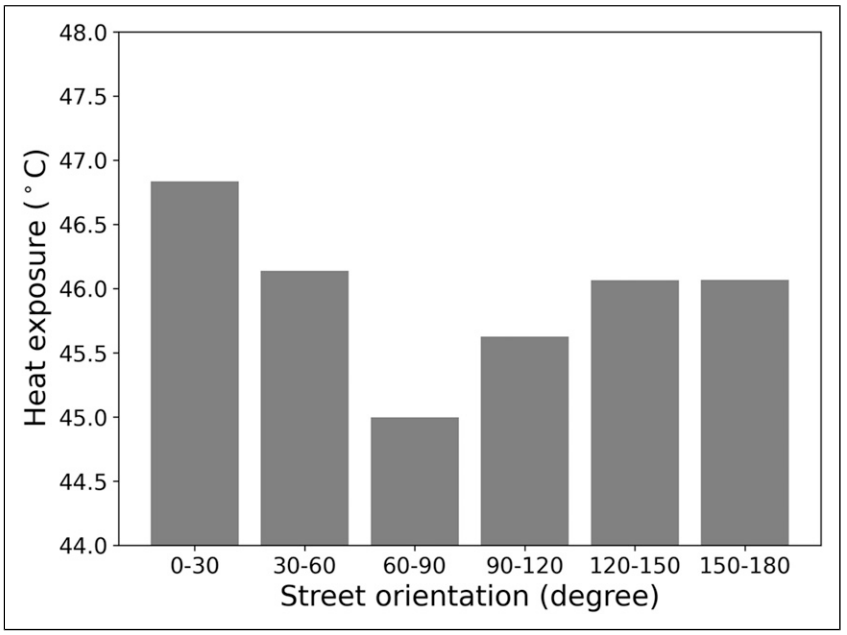

Figure 5. Bar chart of the averaged heat hazard of sidewalks with different orientations (in degrees, start from the east in anti-clockwise way).

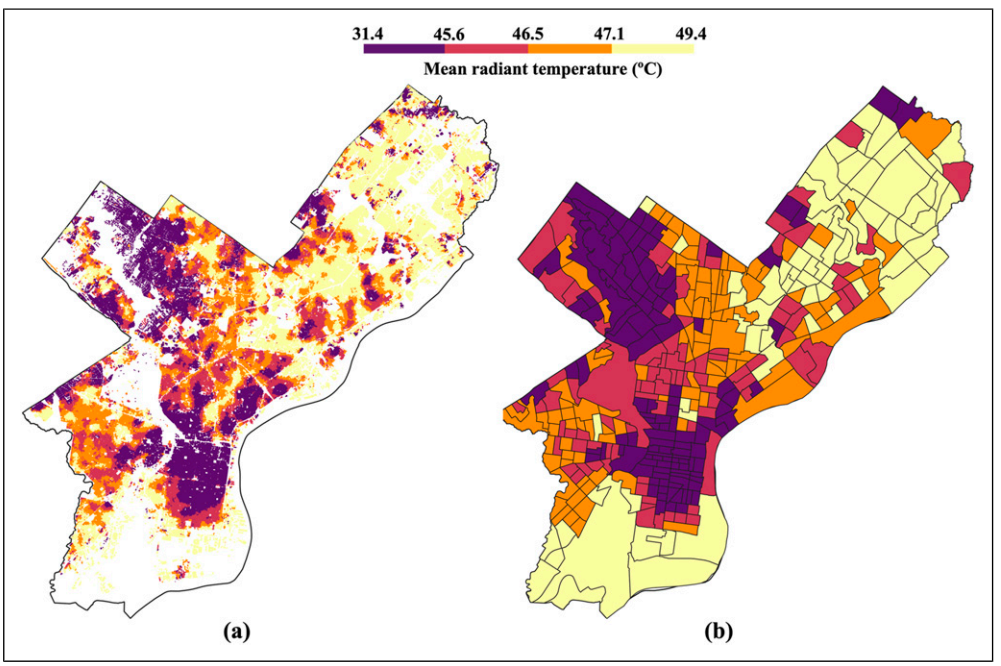

Figure 6. Spatial distribution of the heat hazard within 400m walkshed for each building block: (a) the building level heat hazard within walkshed and (b) the aggregated census tract level heat hazard.

effect. The proportion of Hispanics has no significant association with the building level heat hazard. The proportion of African Americans has a significant and positive association with the building level heat hazard after controlling the spatial effect. The proportion of people under 5 years of age has a significant and positive association with the building level heat hazard in the OLS model, while in the spatial regression model the association is not significant.

Discussion

The study applies geospatial data analytics, urban microclimate modeling, and GPU parallel computing to model and map urban outdoor heat hazard at the pedestrian level. High-resolution (1m) multispectral aerial imageries and LiDAR cloud point data were used to generate the 3D urban fabrics, which were then used to model the radiation fluxes and estimate the mean radiant

Table 2. Correlation coefficients between the aggregated building level heat hazard (mean radiant temperature, T_{mrt}) and the socioeconomic and racial/ethnic variables at the census tract level.

Category	Variables	Pearson's correlation	Sig (2-tailed)	*N*
Economic status	Per capita income	−0.47**	0.000	374
Education	Proportion of people without high school degree	0.42**	0.000	
	Proportion of people with bachelor or higher degrees	−0.59**	0.000	
Race and ethnicity	Proportion of non-Hispanic Whites	−0.36**	0.000	
	Proportion of Hispanics	0.22**	0.000	
	Proportion of African Americans	0.25**	0.000	
	Proportion of Asian Americans	−0.11	0.029	
Age	Proportion of people under 5 years of age	0.34**	0.000	
	Proportion of people older than 65 years of age	−0.07	0.178	

** Correlation is significant at the 0.01 level (2-tailed).

Table 3. Ordinary least squares (OLS) regression model and spatial lag model (SAR_{lag}) of the aggregated building level mean radiant temperature (T_{mrt}) and independent variables at census tract level in the study area.

	OLS	SAR_{lag}
Variables	Coefficients (*z-values*)	Coefficients (*z-values*)
Constant	46.48**	5.49**
Per capita income (thousand dollar)	−0.03 (−5.98**)	−0.002 (−0.098)
Proportion of Hispanics	0.39 (0.72)	0.25 (0.97)
Proportion of African Americans	−0.06 (−0.16)	0.42 (2.48*)
Proportion of Asian Americans	−0.84 (−0.83)	0.66 (1.32)
Proportion of people under 5 years of age	11.70 (4.88**)	0.41 (0.31)
R^2	0.28	
Pseudo R-squared		0.83
Adjusted R^2	0.27	
F-statistic	28.42**	
Moran's I of residuals	0.68 (23.28**)	

**Significant at the 0.01 level (2-tailed).
*Significant at the 0.05 level (2-tailed).

temperature (T_{mrt}) as the indicator of the urban outdoor heat hazard. In doing so, it produces high spatial resolution (1m) urban outdoor heat hazard map for Philadelphia. The fine-resolution heat hazard maps present unprecedented details of the distribution of urban heat across the city with consideration of shading effects of the surrounding fine level urban landscape features. Such hyperlocal information about the spatial distribution heat hazard would help to provide more actionable insights for climate-resilient planning and policies. For example, it provides an efficient tool to examine which neighborhoods, blocks, and streets need more resources for heat mitigations, such as tree planting and shading infrastructure. The high-resolution T_{mrt} can also be incorporated to estimate the heat vulnerability and support the heat management and emergency planning in extreme heat weathers.

By overlaying the sidewalk map on the generated heat hazard map, this study estimated the heat hazard level along sidewalks in Philadelphia. This is the first sidewalk level urban heat mapping at the city scale. The sidewalk level heat hazard map provides a pedestrian level heat hazard spatial distribution in Philadelphia. Generally, the tree canopy cover, height of street trees, and height of buildings all associated with lower heat hazard level. In addition, the orientation of the sidewalk would also impact the heat hazard significantly. Those sidewalks that orient in the degrees of 0 to 30 from the east in anti-clockwise way have higher heat hazard than sidewalks of other orientations in Philadelphia. In this study, the heat hazard is the averaged T_{mrt} from 9a.m. to 4p.m., while the T_{mrt} varies significantly hour by hour. Therefore, this pattern may not be valid at hourly level. In cities of different latitudes, the heat hazard levels of sidewalks with different orientations may be different because of the different sun paths in the summertime.

This study also studied the heat hazard at the building level by estimating the average heat hazard in the 400m walking distance walkshed of each building block. Therefore, the heat hazard in the walkshed can better indicate human potential heat hazard. The building level heat hazard clearly presents the spatial distribution of the potential heat hazard for urban residents in Philadelphia. Generally, the downtown area and the northwestern parts of the city have a lower heat hazard level than the northeastern and northern parts of the city. This study aggregated the building level heat hazard to census tract level and investigated the heat hazard among different socioeconomic and racial/ethnic groups across neighborhoods of Philadelphia. Different from previous work (Li, 2021) that used the aggregated T_{mrt} values of all non-building pixels at the census tract level, the sidewalk level heat hazard has no significant association with income in Philadelphia after controlling the spatial dependence. In addition, the racial/ethnic statuses have a significant association with the sidewalk level heat hazard, as neighborhoods with higher proportion of African Americans tend to have higher sidewalk level heat hazard.

The developed framework in this study provides an objective way to study human heat hazard from a pedestrian perspective in a human-centric way. The developed method is highly scalable and can be easily scaled to other cities in the United States since the datasets used in this study are publicly accessible and nationally available. The generated fine-resolution heat hazard map can be also overlaid with other urban facility maps to examine the heat hazard in other facilities, such as public transit stations, playgrounds, schoolyards, and parks, which seem impossible using traditional methods. The developed study would be applied to examine urban resident's heat hazard more objectively and provide new insights to alleviate the vulnerabilities to the heat through urban climate planning, which are of great importance in the context of climate change and urban heat island intensification.

Although this study examined the heat hazard level in Philadelphia from the pedestrian perspective, there are still several limitations in this study. Firstly, this study only studied the daytime urban outdoor heat hazard level, and the heat hazard at nighttime was not considered. However, the nighttime and indoor heat stress levels also impact human wellbeing significantly. In this study, the walksheds of buildings were used as the surrogate of the human potential walking areas, while the

actual pedestrian's activities were not considered. Using different urban facilities like parks, playgrounds, and bus stops as destinations would be a new option to indicate human potential walking paths. Using the fine-level human mobility data would help to better represent human walking activities and further indicate the heat exposure of pedestrians.

Another limitation of this study is that the 400m walking distance was used as the universal distance to define the walkshed in the whole city to examine heat hazard, while the walking distance may be different in different urban form settings of the study area. Future work should use adaptive distance for different areas in the study area. In addition, this study didn't consider the different land uses of building blocks. However, different types of buildings may have different functions of human activities and different population densities; therefore, future studies should also consider the different functions of buildings and the population density.

In addition, this study used the averaged T_{mrt} at hourly level in the summertime to indicate the heat hazard levels. However, the temporal variation of the heat hazard along the sidewalk was not considered, while the temporal variation of the heat in different time of 1 day is significant. Therefore, future research should consider the heat hazard at the sidewalk and building levels at different time points.

Conclusion

This study examined the spatial distributions of heat hazard from pedestrian perspective at sidewalk and building level using urban microclimate modeling based on 1m resolution urban geometrical model. The existence of the street trees and buildings would help to lower the heat hazard level along sidewalk. The orientations of the sidewalk impact the heat hazard of sidewalk significantly, while the relationship varies at different hours, days, and spatial locations. Social-environmental analysis results show that neighborhoods with a higher proportion of African Americans have a higher heat hazard level in Philadelphia.

This study presents a scalable and efficient tool to evaluate the heat hazard at the sidewalk and building block level from a more human-centric perspective at the city scale. Such a developed human-centric framework for estimating pedestrian level heat hazard would provide a powerful tool for developing more thermally comfortable and pedestrian-friendly cities in the context of climate change.

Declaration of conflicting interests

The author(s) declared no potential conflicts of interest with respect to the research, authorship, and/or publication of this article.

Funding

The author(s) disclosed receipt of the following financial support for the research, authorship, and/or publication of this article: This work was supported by the National Science of Foundation, 2314709.

ORCID iD

Xiaojiang Li https://orcid.org/0000-0002-4208-1641

Data Availability Statement

The datasets generated during and/or analyzed during the current study are available from the corresponding author on reasonable request.

References

Alexander LV and Arblaster JM (2009) Assessing trends in observed and modelled climate extremes over Australia in relation to future projections. *International Journal of Climatology* 29(3): 417–435.

Borden KA and Cutter SL (2008) Spatial patterns of natural hazards mortality in the United States. *International Journal of Health Geographics* 7(1): 64.

Easterling DR, Meehl GA, Parmesan C, et al. (2000) Climate extremes: observations, modeling, and impacts. *Science* 289(5487): 2068–2074.

Gabriel KMA and Endlicher WR (2011) Urban and rural mortality rates during heat waves in Berlin and Brandenburg, Germany. *Environmental Pollution* 159(8–9): 2044–2050.

Hsu A, Sheriff G, Chakraborty T, et al. (2021) Disproportionate exposure to urban heat island intensity across major US cities. *Nature Communications* 12(1): 2721.

Karner A, Hondula DM and Vanos JK (2015) Heat exposure during non-motorized travel: implications for transportation policy under climate change. *Journal of Transport & Health* 2(4): 451–459.

Klemm W, Heusinkveld BG, Lenzholzer S, et al. (2015) Street greenery and its physical and psychological impact on thermal comfort. *Landscape and Urban Planning* 138: 87–98.

Kong F, Chen J, Middel A, et al. (2022) Impact of 3-D urban landscape patterns on the outdoor thermal environment: a modelling study with SOLWEIG. *Computers, Environment and Urban Systems* 94: 101773.

Landry SM and Chakraborty J (2009) Street trees and equity: evaluating the spatial distribution of an urban amenity. *Environment and Planning A* 41(11): 2651–2670.

Lee H, Holst J and Mayer H (2013) Modification of human-biometeorologically significant radiant flux densities by shading as local method to mitigate heat stress in summer within urban street canyons. *Advances in Meteorology* 2013: 1–13.

Li X (2021) Investigating the spatial distribution of resident's outdoor heat exposure across neighborhoods of Philadelphia, Pennsylvania using urban microclimate modeling. *Sustainable Cities and Society* 72: 103066.

Li X and Wang G (2021) GPU parallel computing for mapping urban outdoor heat exposure. *Theoretical and Applied Climatology* 145: 1101–1111.

Li R, Chester MV, Hondula DM, et al. (2023) Repurposing mesoscale traffic models for insights into traveler heat exposure. *Transportation Research Part D: Transport and Environment* 114: 103548.

Lindberg F and Grimmond CSB (2011) The influence of vegetation and building morphology on shadow patterns and mean radiant temperatures in urban areas: model development and evaluation. *Theoretical and Applied Climatology* 105(3): 311–323.

Lindberg F, Holmer B and Thorsson S (2008) SOLWEIG 1.0–Modelling spatial variations of 3D radiant fluxes and mean radiant temperature in complex urban settings. *International Journal of Biometeorology* 52: 697–713.

Maronga B, Gryschka M, Heinze R, et al. (2015) The Parallelized Large-Eddy Simulation Model (PALM) version 4.0 for atmospheric and oceanic flows: model formulation, recent developments, and future perspectives. *Geoscientific Model Development* 8(8): 2515–2551.

Matzarakis A, Rutz F and Mayer H (2007) Modelling radiation fluxes in simple and complex environments—application of the RayMan model. *International Journal of Biometeorology* 51(4): 323–334.

McPhearson T, Mustafa A and Ortiz L (2020) Heat and coronavirus can be twin killers. *Nature* 582(7810): 32–33.

Norton BA, Coutts AM, Livesley SJ, et al. (2015) Planning for cooler cities: a framework to prioritise green infrastructure to mitigate high temperatures in urban landscapes. *Landscape and Urban Planning* 134: 127–138.

Patz JA, Campbell-Lendrum D, Holloway T, et al. (2005) Impact of regional climate change on human health. *Nature* 438(7066): 310–317.

Reid CE, O'neill MS, Gronlund CJ, et al. (2009) Mapping community determinants of heat vulnerability. *Environmental Health Perspectives* 117(11): 1730–1736.

Rey SJ and Anselin L (2009) PySAL: a Python library of spatial analytical methods In: *Handbook of Applied Spatial Analysis: Software Tools, Methods and Applications*. Berlin, Heidelberg: Springer Berlin Heidelberg, 175–193.

Stone B, Hess JJ and Frumkin H (2010) Urban form and extreme heat events: are sprawling cities more vulnerable to climate change than compact cities? *Environmental Health Perspectives* 118(10): 1425–1428.

Xiaojiang Li is a tenure-track assistant professor at Department of City and Regional Planning, University of Pennsylvania. He is also the co-founder of ***Biometeors***. He was a Postdoctoral Fellow at MIT Senseable City Lab. His research focuses on developing and applying geospatial analyses and data-driven approaches in the domain of urban studies. He has proposed to use Google Street View for urban environmental studies and developed the Treepedia project, which aims to map street greenery for cities around the world. He is working on ***HeatExpo*** using artificial intelligence, remote sensing, urban microclimate modeling, and urban analytics to investigate the different vulnerabilities to climate change across different neighborhoods in the U.S. He is also working on using human trace data to study human activities and investigate the connection between urban environments and human activities.